AGU PUBLICATIONS

JGR

Journal of Geophysical Research: Space Physics

RESEARCH ARTICLE

10.1002/2014JA019842

Key Points:
- Two-spacecraft ARTEMIS mission explores lunar dayside environment in the lobe
- Interspacecraft magnetic differences infer presence of field-aligned current
- Both electrons and lunar heavy ions contribute significantly to the current

Correspondence to:
X.-Z. Zhou,
xuzhi.zhou@gmail.com

Citation:
Zhou, X.-Z., V. Angelopoulos, A. R. Poppe, J. S. Halekas, K. K. Khurana, M. G. Kivelson, S. Fatemi, and M. Holmström (2014), Lunar dayside current in the terrestrial lobe: ARTEMIS observations, *J. Geophys. Res. Space Physics*, *119*, doi:10.1002/2014JA019842.

Received 31 JAN 2014
Accepted 21 APR 2014
Accepted article online 24 APR 2014

Lunar dayside current in the terrestrial lobe: ARTEMIS observations

X.-Z. Zhou[1,2], V. Angelopoulos[1,2], A. R. Poppe[3], J. S. Halekas[3], K. K. Khurana[1,2], M. G. Kivelson[1,2], S. Fatemi[4], and M. Holmström[4]

[1]Department of Earth, Planetary, and Space Sciences, University of California, Los Angeles, California, USA, [2]Institute of Geophysics and Planetary Physics, University of California, Los Angeles, California, USA, [3]Space Science Laboratory, University of California, Berkeley, California, USA, [4]Swedish Institute of Space Physics, Kiruna, Sweden

Abstract We report Acceleration, Reconnection, Turbulence and Electrodynamics of Moon's Interaction with the Sun (ARTEMIS) dual-probe observations of two events in the terrestrial magnetotail lobe, both characterized by upward moving heavy ions of lunar origin at one of the probes that is magnetically connected with the dayside lunar surface. By treating magnetic measurements at the other probe as the unperturbed lobe fields, we obtain background-subtracted magnetic perturbations (most significantly in B_z) when the first probe moved in the dawn-dusk direction across flux tubes magnetically connected to the Moon. These magnetic perturbations indicate the presence of field-aligned current above the lunar surface. By examining possible carriers of field-aligned current, we find that lunar heavy ions and accompanying electrons both contribute considerably to the current. Observations of the field-aligned current also suggest that the charging process at the dayside lunar surface and the associated lobe plasma environment, which have traditionally been viewed as a one-dimensional current balance problem, are actually more complicated. These observations give the first insights into how heavy ions affect the lunar dayside environment in terms of multispecies plasma dynamics.

1. Introduction

The lunar surface, enveloped only by a very tenuous exosphere and not protected by a global intrinsic magnetic field, is exposed to the space plasma environment and is therefore continuously bombarded by incident charged particles from the solar wind and/or the terrestrial magnetotail. The dayside lunar surface is also illuminated by solar ultraviolet radiation that stimulates photoelectron emissions. Both mechanisms contribute to charge transfer between the Moon and its ambient plasma environment. Lunar surface charging (much like spacecraft charging) has been treated as a simple one-dimensional current balance problem [e.g., *Goldstein*, 1974; *Farrell et al.*, 2013; *Stubbs et al.*, 2014] because the lunar radius is significantly greater than the typical Debye scale; charge transfer will proceed until an equilibrium is reached and the net current to the lunar surface becomes zero [*Whipple*, 1981].

By analyzing different sources of surface-charging currents, including the incident particles and the escaping secondary electrons and photoelectrons, a number of studies have been carried out to theoretically understand the equilibrium and to determine the associated electrostatic potential profile [*Guernsey and Fu*, 1970; *Fu*, 1971; *Walbridge*, 1973; *Nitter et al.*, 1998]. Depending on the photoelectron and ambient electron properties, the resultant electrostatic potential profile could be either monotonic or nonmonotonic (with a minimum above the sunlit lunar surface). This idea has been supported by spacecraft observations [*Halekas et al.*, 2008, 2011; *Poppe et al.*, 2011] and particle-in-cell simulations [*Poppe and Horányi*, 2010; *Farrell et al.*, 2013]. According to these simulations, the one-dimensional equilibrium can be established very quickly (within few electron plasma periods).

The aforementioned studies, however, have not taken into account the possible effects of lunar heavy ions [*Hilchenbach et al.*, 1993; *Mall et al.*, 1998; *Tanaka et al.*, 2009; *Yokota et al.*, 2009; *Poppe et al.*, 2012; *Harada et al.*, 2013; *Zhou et al.*, 2013]. Generated mostly via photoionization of lunar surface and/or exospheric neutrals, these ions could be picked up by the ambient plasma and at the same time accelerated by the near-surface electric field, thereby contributing to the charging currents. Lunar heavy ions have been also observed to be accompanied by cold electrons (with density over 10 times greater than the background lobe population) to maintain charge quasi-neutrality beyond the Debye scale [*Harada*

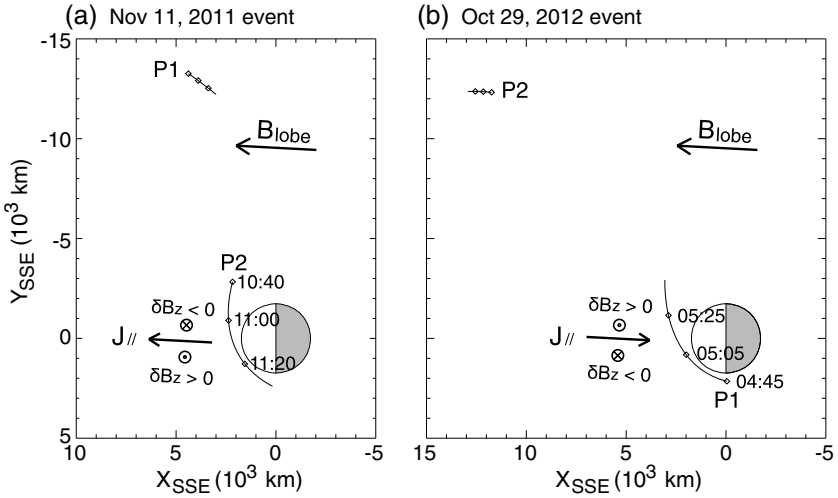

Figure 1. Acceleration, Reconnection, Turbulence and Electrodynamics of Moon's Interaction with the Sun (ARTEMIS) P1 and P2 trajectories with respect to the Moon during the (a) 11 November 2011 and the (b) 29 October 2012 events, in the *XY* plane of the Selenocentric Solar Ecliptic (SSE) coordinates (where the *X* axis points from the Moon to the Sun, the *Z* axis points toward the ecliptic north pole, and the *Y* axis completes the right-handed set of axes). During these events, the Moon was located in the Earth's magnetotail at GSE [−62.5, −7.5, 2.0] and [−62.6, 7.5, 2.6] R_E, respectively. Also shown are the directions of the background lobe field, the magnetic perturbations associated with the lunar flybys, and the inferred field-aligned current.

et al., 2013; *Zhou et al.*, 2013]; the roles of these electrons on the current balance problem remains unclear as well.

In this paper, we present two events observed by the dual-probe lunar-orbiting ARTEMIS mission [*Angelopoulos*, 2011]. In both events, heavy ions of lunar origin were observed at one of the probes, which was magnetically connected with the dayside lunar surface in the terrestrial lobe. The background environment of the lobe region was measured by the other ARTEMIS probe located nearby (see Figure 1 for the ARTEMIS equatorial orbits with respect to the Moon in these two events). Given the quasi-uniform magnetic field in the lobe region with negligible current, the interspacecraft magnetic differences provide important information regarding the current associated with the lunar space environment. These two events will be accordingly studied in terms of these currents and their carriers, after we briefly introduce the ARTEMIS instruments we use in the next section.

2. Instrumentation

The ARTEMIS mission [*Angelopoulos*, 2011], an extension of the five-probe Time History of Events and Macroscale Interactions during Substorms (THEMIS) mission [*Angelopoulos*, 2008], redeployed two of the THEMIS probes (P1 and P2) to elliptical equatorial orbits around the Moon. Each ARTEMIS probe carries identical instrumentation. In this study, data from the following instruments are used: (1) the Fluxgate Magnetometer (FGM) [*Auster et al.*, 2008], which provides DC magnetic field measurements; (2) the Electric Field Instrument (EFI) [*Bonnell et al.*, 2008], which measures electric field and the spacecraft potential; and (3) the electrostatic analyzer (ESA) [*McFadden et al.*, 2008a], the highly sensitive plasma instrument that measures the three-dimensional ion and electron distribution functions in the energy range from a few eV up to 25 keV.

ESA does not resolve ion mass, however. In the presence of lunar heavy ions, the usual assumption that all observed ions are protons becomes invalid. Given an average ion mass of *M* amu, the assumption that all ions are protons overestimates the ion velocity by a factor of $\sqrt{M}$ (the energy of each ion is correctly measured), and also underestimates the ion number density by the same factor of $\sqrt{M}$ [*McFadden et al.*, 2008b]. Note that these two factors compensate when the first-order moment of the measured ion distribution function (which equals the ion bulk velocity multiplied by density) is computed. The computation of the ion current density from ESA measurements, therefore, does not depend on *M*. Before the

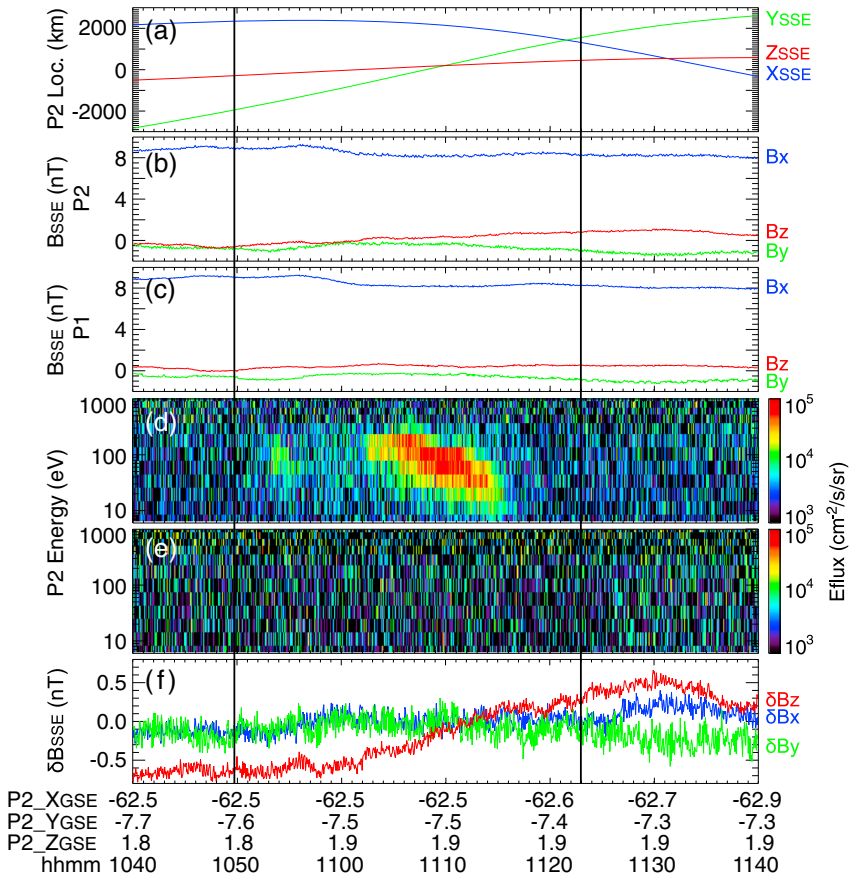

Figure 2. A 1 h overview of ARTEMIS P2 and P1 observations on 11 November 2011. (a) ARTEMIS P2 location in SSE coordinates; (b) magnetic field components at P2 in SSE coordinates; (c) magnetic components in SSE coordinates at P1, which represent the background lobe field; (d and e) ion energy spectra at P2 in the earthward (upward) and tailward (downward) directions, respectively; and (f) magnetic field differences between P2 and P1 measurements.

computation, we need only adjust the measured energy of each ion (spacecraft potential Φ_{sc} added) so that the ion deceleration by positive spacecraft charging is taken into account.

3. The 11 November 2011 Event

Figure 2 provides a 1 h overview of ARTEMIS P2 and P1 observations on 11 November 2011 when the Moon was located in the Earth's magnetotail at GSE [−62.5, −7.5, 2.0] R_E (R_E: Earth radius, or 6371 km). During this time interval, ARTEMIS P2 was near its periapsis (~300 km above the dayside lunar surface) moving duskward, and P1 was ~12,000 km dawnward of P2 (see Figures 1a and 2a). The magnetic fields measured at P2 and P1, shown in Figures 2b and 2c, respectively, were both predominantly in the *X* (earthward) direction. The B_x dominance, together with the low plasma beta (~0.05 at 1050 UT, not shown), suggests that both probes were located in the northern lobe region. The quasi-steady magnetic measurements also indicate the absence of any obvious magnetic structures such as plasmoids or traveling compression regions [e.g., *Slavin et al.*, 1984, 1999; *Li et al.*, 2013]. The B_x-dominated lobe field lines connected P2 with the underlying lunar surface during the time interval bounded by the two vertical lines in Figure 2 (under the straight-field-line approximation).

This event has been previously reported [*Poppe et al.*, 2012, 2013; *Zhou et al.*, 2013] in the context of lunar pickup ions observed at P2 and their mass estimations (~28 amu). Figure 2d shows the ion differential energy fluxes at P2 in the earthward direction (away from the Moon), in which these heavy ions were found at energies below 200 eV from 1053 to 1056 UT and more significantly from 1102 to 1117 UT. During both intervals, P2 was magnetically connected with the underlying dayside lunar surface. Note that the tailward (downward) ion fluxes shown in Figure 2e remained unchanged at background (lobe) levels. According to

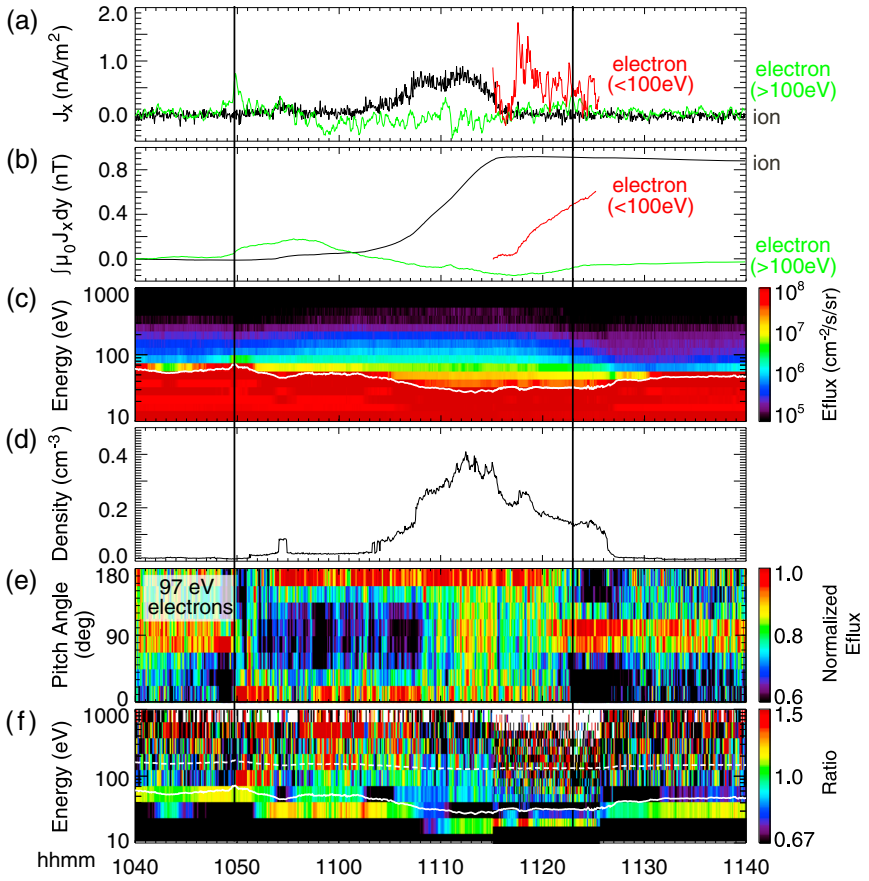

Figure 3. ARTEMIS P2 observations of (a) field-aligned currents in the earthward direction and (b) integrations of these currents over *Y*; (c) omnidirectional electron energy spectra, with the white line representing the spacecraft potential Φ_{sc}; (d) plasma density, adopted from *Zhou et al.* [2013]; (e) electron pitch angle spectra at the 97 eV energy channel, normalized at each time sample by the maximum flux in any direction; and (f) ratio between earthward and tailward electron fluxes at different energies, with the solid and the dashed white lines representing Φ_{sc} and Φ_{sc}+ 100 eV, respectively.

Poppe et al. [2013], the upward motion of these pickup ions is mainly attributed to the upward photoelectric field near the lunar surface.

To discuss the magnetic perturbations associated with these observations, as previously suggested, we treat the magnetic measurements at P1 as the background lobe field and subtract them from their counterparts at P2. In the absence of any obvious magnetic structures at either probe, the resultant interspacecraft magnetic difference $\delta\mathbf{B}$ (shown in Figure 2f) can be interpreted as the background-subtracted magnetic field at P2. It should be noted that the resultant $\delta\mathbf{B}$ values could be biased, especially in the *Z* direction due to the magnetic offsets that could reach 0.5–1 nT at both P1 and P2. However, given that the offsets could only drift ~0.1 nT during the interval of interest (U. Auster and F. Plaschke, private communication, 2014), the variations of the measured $\delta\mathbf{B}$ are still reliable. As P2 moved duskward over the dayside lunar surface, the δB_z values gradually increased by ~1 nT (the other two components varied very slightly), which indicates the presence of an earthward, field-aligned current.

Although it is widely believed that electrons are more typical carriers of field-aligned currents because of their high mobility, the observed coincidence between the field-aligned current and the upward-moving ions suggests that these heavy ions of lunar origin could also be carriers of such currents. To understand the relative contribution of these heavy ions to the dayside field-aligned current system, we compute the first-order moment of the measured ion distribution function to obtain the ion-carried current density (which does not depend on ion mass, as discussed in section 3). The resultant ion-carried current density in the earthward (field-aligned) direction is shown in Figure 3a as the black line.

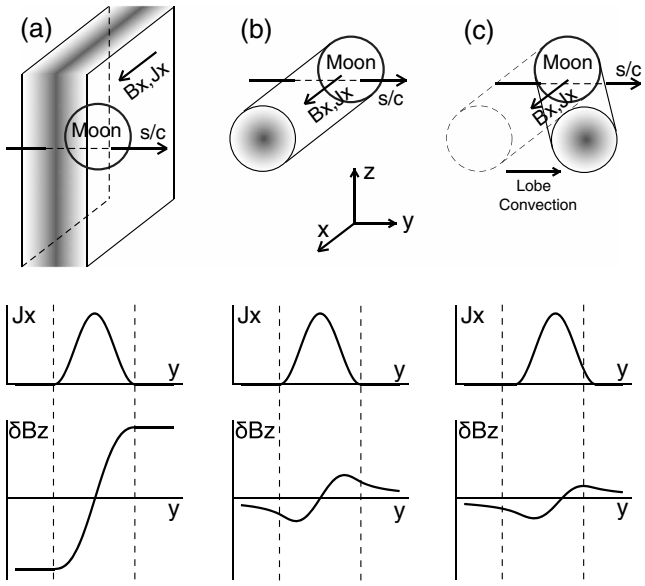

Figure 4. Possible lunar dayside current configurations and their associated equatorial current J_x and magnetic B_z profiles. The shaded region depicts the spatial extent of J_x, and the gray scale indicates the current density. (a) Planar, infinite current sheet model in which J_x and B_z depend only on Y; (b) centrosymmetric and (c) tilted cylindrical-type current models with similar equatorial J_x profiles but much weaker B_z variations than the sheet model.

To determine the magnetic B_z perturbations caused by the observed field-aligned ion current, we next integrate the ion current density $J_{i,x}$ over Y, represented by the black line in Figure 3b. The resultant profile, including its enhancement of ~0.9 nT, apparently agrees with the background-subtracted magnetic B_z measurements (shown in Figure 2f).

It should be kept in mind, however, that the Y integration of J_x does not equal δB_z unless the current flows in a planar, infinite sheet parallel to the XZ plane (so J_x and δB_z only depend on Y, see Figure 4a). This is very unlikely to be the case, even if the real configuration of the dayside current system remains unclear, because one cannot expect the observed near-equatorial current to also be present at large Z locations with the same intensity. In other words, the magnetic perturbation associated with the observed ion current must be less significant than its Y integration shown in Figure 3b due to the expected weaker current at higher latitudes.

If we assume that lunar ions can stream only along magnetic field lines (neglecting the effects of magnetotail convection), the resultant ion current would appear only at locations magnetically connected with the dayside lunar surface (a centrosymmetric, cylindrical-type configuration with the axis approximately in the X direction), and the amplitude of the magnetic perturbation (see Figure 4b) would be approximately one third of the magnetic perturbation calculated for a planar, infinite current sheet. In the presence of magnetotail convection, ions of lunar origin would be picked up by the convective electric field and therefore be distributed in a broad wedge on one side of the Moon [see *Poppe et al.*, 2013, Figure 3a]. Ions with small pitch angles (that can carry field-aligned currents), however, would still be approximately confined to a cylinder tilted in the same direction as lobe convection [see *Poppe et al.*, 2013, Figure 3d]. A low-altitude spacecraft flyby would observe a J_x profile similar to that in Figure 4b (only shifted slightly in the direction of convection, see Figure 4c), and the associated magnetic perturbation would again be approximately one third of the magnetic perturbation under the infinite current sheet assumption.

In other words, we expect that only part of the upward field-aligned current associated with the observed magnetic perturbation was carried by the upward moving lunar ions. The other part of the current, with intensity likely twice as large as the ion current, must be carried by electrons with higher fluxes in the tailward direction toward the Moon. This electron current could arise from lunar blockage of earthward electron flux at high energies [*Halekas et al.*, 2011], although high-energy electrons were rare in the lobe. The other possible current carriers are cold electrons (with density significantly enhanced and temperature reduced to ~20 eV), which accumulate to accompany the lunar heavy ions and satisfy the plasma quasi-neutrality requirement [*Zhou et al.*, 2013]. To distinguish between these two different sources, we next integrate the measured distribution function of electrons below and above 100 eV separately, to compute the densities of current carried by cold and hot electrons, respectively.

Computation of the current density carried by electrons at higher energies (above 100 eV) is straightforward. Before integrating the measured electron distribution function, we need only subtract the spacecraft potential Φ_{sc} from the measured energy of each electron to take into account the acceleration from spacecraft charging. Computation of the current density carried by low-energy electrons, on the other hand, is

more difficult because of contamination from spacecraft-generated photoelectrons. Figure 3c shows the electron energy spectrum, in which the spacecraft-generated photoelectrons can be clearly seen with very high fluxes at energies lower than the spacecraft potential Φ_{sc} (white line). Ambient electrons, which had been accelerated by positive spacecraft charging before being recorded, appeared at energies above Φ_{sc} with enhanced fluxes (still lower than photoelectron fluxes) from 1102 to 1125 UT. The separation of the two populations is not completely clean [*McFadden et al.*, 2008b], however, because the measurement at energy channels just above Φ_{sc} could be heavily contaminated by spacecraft-generated photoelectrons. Therefore, it is important to remove these photoelectrons in the computation of cold electron-carried current density.

The contamination-removal method, successfully applied to obtain the electron density for the same event [*Zhou et al.*, 2013], is used here for each viewing direction before the current density is computed. Only those energy channels with lower boundaries at least a half-channel-width higher than Φ_{sc} are preserved, and the resultant energy gap is filled with extrapolations (logarithmic in phase space density and linear in energy) from measurements at adjacent higher-energy channels. This method, however, is successful with particle-burst data (available from 1115 to 1126 UT) but not with other ESA data products (full and reduced packets, see *McFadden et al.* [2008a]). The reduced packets provide omnidirectional electron spectra that enable computation of the electron density (as done in *Zhou et al.* [2013]) but not velocity; the full packets, on the other hand, have sufficient angular resolution (with 88 solid angles) but insufficient energy resolution (with 15 energy channels, rather than 32 as in the burst and the reduced packets) to be used to calculate current density. The large energy channel widths in the full packets, together with the low temperature (< 20 eV) of the ambient electrons when the lunar ions were present [*Zhou et al.*, 2013], suggests that the data counts be very low (or zero in many directions) even at the second lowest preserved energy channels, which invalidates the logarithmic extrapolation scheme.

Therefore, the density of low-energy electron-carried current can only be accurately computed during the particle-burst interval; in Figure 3, compare the low-energy electron-carried current density (red line) with the current carried by electrons at higher energies (green line). The weak current carried by high-energy electrons, probably caused by scarcity of high-energy electrons in the lobe, suggests that electron lunar blockage played little role in supplying earthward field-aligned current for this event. On the other hand, the current carried by low-energy electrons (at least during the particle-burst interval) was stronger than that carried by high-energy electrons, which suggests that the electron current was mostly carried by electrons below 100 eV. Also, as expected, the current was in the earthward direction with slightly larger intensities than the maximum ion current. The *Y* integration of the low-energy electron current, shown as the red line in Figure 3b, corresponds to a 0.6 nT B_z enhancement within the 10 min particle-burst interval. This enhancement is comparable to the *Y* integration of the ion current during the entire lunar-crossing interval.

We next study the anisotropic features of current-carrying low-energy electrons, by examining the pitch angle distributions of the normalized electron fluxes in the 97 eV energy channel (shown in Figure 3e). These electrons, after energy correction (subtracting Φ_{sc}), were in the 40–90 eV energy range during the 1107–1126 UT interval (when the spacecraft potential was ~30 V, see Figure 3c) and were at lower energies at other times. Pitch angle distributions show higher electron fluxes at pitch angles near 0° and 180° when the probe was magnetically connected with the Moon. The dominance of $\sim 0°$ pitch angles among upward moving electrons could be explained by surface absorption of high pitch angle electrons soon after they were photoemitted from the lunar surface (i.e., the cyclotron shadowing effect for oblique magnetic configurations, see *Harada et al.* [2013]). On the other hand, the fluxes of downward moving electrons were even higher most of the time, especially in the 1107–1123 UT interval when the electron density (in Figure 3d) was relatively high, which agrees with the expectation that the current carried by low-energy electrons was in the earthward direction.

Figure 3f shows the ratio between electron fluxes in the earthward (pitch angle less than 30°) and tailward (pitch angle greater than 150°) directions at different energies (the higher energy resolution of the particle-burst data can be clearly seen in the figure). To avoid being misled by photoelectron contamination, we focus on energy channels above and not adjacent to Φ_{sc} (white solid line). The ratio shows noisy patterns at energies above $\Phi_{sc} + 100$ eV (white dashed line) because of the very low counts, which agree with the negligible current carried by warmer electrons. More consistent patterns can be seen at lower energies (especially within the high plasma density interval from 1107 to 1123 UT) with the ratio typically between 0.8 and 1. The very different distributions between the major current carriers, cold and weakly

anisotropic for electrons and by contrast exclusively earthward for heavy ions, largely compensate the big mass difference between electrons and heavy ions. Therefore, these different anisotropic features justify the observations that heavy ions can also carry a considerable portion of the field-aligned current despite the widespread expectation that highly mobile electrons should be the only carriers of field-aligned current in any space plasma environment.

4. The 29 October 2012 Event

On 29 October 2012 at ~0455 UT, the Moon was in the terrestrial magnetotail at GSE [−62.6, 7.5, 2.6] R_E when ARTEMIS P1 started to move dawnward (rather than duskward as in the previous event, see Figure 1b) above the dayside lunar surface. ARTEMIS P1's position relative to the Moon is also shown in Figure 5a, and P2 was ~18,000 km away from P1 in the dawnward and earthward direction (see Figure 1b). The magnetic measurements at P1 and P2, shown in Figures 5b and 5c, respectively, were again quasi-steady with predominant earthward B_x components suggesting that P1 and P2 were both in the northern lobe (plasma beta ~0.06 at 0455 UT) without observing any significant magnetic structures. During the time interval bounded by the two vertical lines, P1 was magnetically connected with the Moon.

Figures 5d and 5e show P1 observations of the ion differential energy fluxes in the earthward (upward) and tailward (downward) directions, respectively. The heavy ions of lunar origin, once again, were found moving earthward at the energy range of 50–300 eV from 0458 to 0513 UT (within the interval of magnetic connection between P1 and the Moon). The density of field-aligned current carried by these earthward moving ions, computed using the same method as used for the previous event, is represented by the black line in Figure 5g. The earthward current density peaked at ~ 0.5 nA/m^2, about the same intensity as in the previous event.

We also compute the density of the electron-carried field-aligned current. The current carried by electrons at energies above 100 eV (after Φ_{sc} subtraction), represented by the green line in Figure 5g, was also in the earthward direction with greater intensities than the ion current when P1 was magnetically connected with the Moon. Without considering the current carried by electrons below 100 eV, one may expect a decreasing magnetic B_z associated with the earthward field-aligned current as P1 moved dawnward above the lunar surface. However, the background-subtracted δB_z, shown in Figure 5f, generally increased (despite some fluctuations) rather than decreased during the lunar-connected interval. In other words, the net field-aligned current should be downward; the low-energy electrons had to be moving in the upward direction, with the associated downward current intensities greater than the upward ion and high-energy electron currents combined.

As in the previous event, the density of the current carried by low-energy electrons below 100 eV could only be computed during the particle-burst interval, shown in Figure 5g as the red line. Unfortunately, P1 stopped collecting particle-burst data soon after it became magnetically connected with the Moon. Nevertheless, the expected downward current carried by low-energy electrons can still be seen near the end of the particle-burst interval (at ~ 0455) when P1's connection with the Moon began.

The electron energy spectrum (Figure 5h), the normalized pitch angle spectrum (Figure 5i), and the earthward-tailward flux ratio (Figure 5j) were also used to infer the directions of electron motion at various energies. For electrons above 100 eV (the dashed line in Figure 5j, after Φ_{sc} subtraction), tailward moving electrons dominated during the entire lunar-connected interval, which agrees with the observed earthward current and must be caused by lunar blockage of earthward moving electrons. Despite the lunar blockage effect, at energies below 100 eV, the earthward moving electron fluxes were higher than the tailward fluxes (also see Figure 5i for normalized electron pitch angle spectrum), which qualitatively agrees with the expectation of downward current carried by low-energy electrons. The ratio became even larger from 0520 to 0534 UT, which corresponds to the interval when δB_z increased more rapidly. These electrons, which moved upward despite the positive surface potential, were most likely in the high-energy tail of the lunar-emitted photoelectron distribution.

5. Comparisons With Nonlunar Lobe Events

In the two events studied, interspacecraft magnetic differences δB_z are treated as background-subtracted B_z perturbations. It should be kept in mind that this approach, together with its implications for the

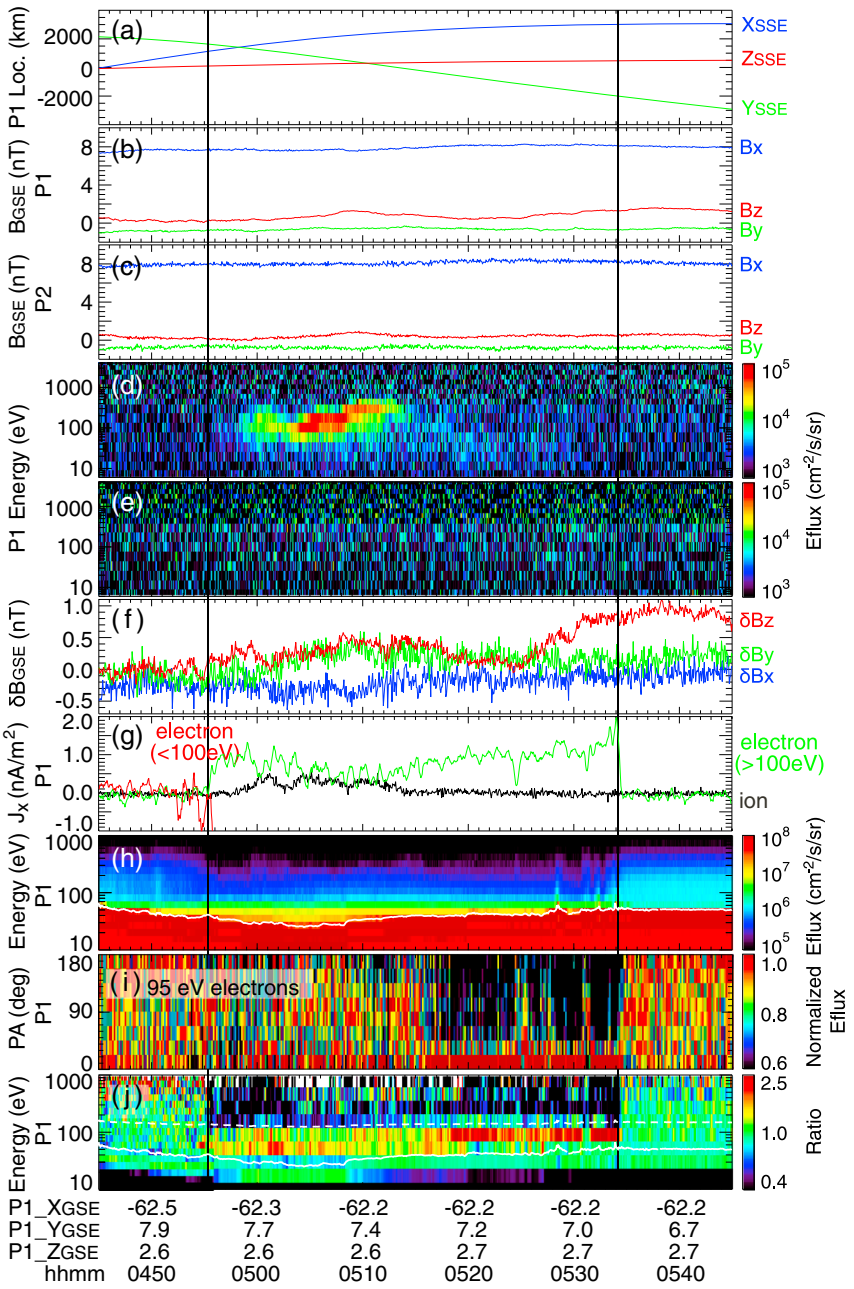

Figure 5. A 1 h overview of ARTEMIS P1 and P2 observations on 29 October 2012. (a) ARTEMIS P1 location in SSE coordinates; (b and c) magnetic fields in SSE coordinates at P1 and P2, respectively; (d) earthward and (e) tailward ion energy spectra at P1; (f) differences between magnetic fields at P1 and P2; (g) field-aligned current in the earthward direction; (h) omnidirectional electron energy spectra; (i) normalized electron pitch angle spectra at the 95 eV channel; and (j) ratio between earthward and tailward electron fluxes. The solid and the dashed white lines correspond to Φ_{sc} (the spacecraft potential) and $\Phi_{sc} + 100$ eV, respectively.

lunar-associated field-aligned current, is based on the assumption that the lobe field is quasi-uniform so δB_z variations do not arise from nonlunar structures and/or fluctuations.

This assumption, which is largely supported by the absence of obvious magnetic structures such as plasmoids or traveling compression regions in these two events, will be further examined by statistically studying δB_z variation levels in nonlunar lobe events. To select these events, we used ARTEMIS observations (2 years, from September 2011 to September 2013) to find all time intervals longer than 1 h when P1 and P2 both stayed in the lobe (plasma beta smaller than 0.1) and were reasonably far from the Moon ($|Y_{SSE}|$ greater

Table 1. List of Nonlunar Lobe Events

Event #	Date	Interval Midpoint	σ_{Bx} at P1 (nT)	σ_{Bx} at P2 (nT)	$\sigma_{\delta Bz}$ (nT)
1	2011-11-10	23:05:23	0.30	0.26	0.15
2	2011-11-11	06:00:27	0.46	0.49	0.16
3	2011-11-11	08:20:46	0.52	0.51	0.12
4	2012-04-06	21:18:12	0.66	0.61	0.25
5	2012-04-06	23:26:40	0.43	0.43	0.11
6	2012-04-07	01:57:17	0.28	0.30	0.09
7	2012-04-07	05:48:47	0.26	0.27	0.05
8	2012-04-07	08:46:24	0.47	0.46	0.08
9	2012-04-08	02:18:03	0.76	0.79	0.14
10	2012-05-05	17:55:00	0.26	0.25	0.05
11	2012-05-05	20:21:05	0.12	0.12	0.07
12	2012-05-06	11:49:37	0.16	0.15	0.08
13	2012-05-06	13:21:36	0.69	0.69	0.08
14	2012-06-03	04:35:38	0.26	0.28	0.09
15	2012-06-04	04:30:21	0.47	0.44	0.09
16	2012-10-29	08:29:13	0.43	0.44	0.13
17	2013-02-23	22:25:56	0.40	0.39	0.22
18	2013-02-24	01:41:02	0.23	0.22	0.13
19	2013-02-24	03:05:00	0.24	0.23	0.13
20	2013-02-26	06:10:55	0.74	0.64	0.21
21	2013-02-26	10:17:01	0.70	0.70	0.13
22	2013-08-21	07:39:27	0.92	1.16	0.33
23	2013-08-21	11:31:43	0.28	0.28	0.15

than 8000 km). To ensure proper comparison, B_x fluctuation levels within each interval were required to be similar to those in the two benchmark lunar flybys: the time derivative of the 60 s running-averaged B_x must not exceed 0.01 nT/s in absolute value at both P1 and P2 (the maximum $|dB_x/dt|$ values at P1 and P2 were 0.005 and 0.009 nT/s, respectively, for the 11 November event, and 0.004 and 0.009 nT/s, respectively, for the 29 October event).

Twenty-three events meet these criteria, and the midpoint of each event interval is listed in Table 1. We next compute the interspacecraft magnetic differences δB_z for all identified nonlunar lobe events. From each event, we select the centermost 1 h interval to obtain the B_x standard deviations σ_{Bx} at P1 and P2 (used to characterize the lobe field variations), as well as the δB_z standard deviations $\sigma_{\delta Bz}$ also listed in Table 1.

The parameters listed in Table 1 are then used to construct Figure 6, in which the abscissa and ordinate of each plus sign are the σ_{Bx} (average of P1 and P2 data) and $\sigma_{\delta Bz}$ values of each nonlunar lobe event. The relatively low $\sigma_{\delta Bz}$ values suggest that the magnetic B_z observed at P1 and P2 are generally well correlated, which is consistent with the negligible current expected in the lobe region. Also as expected, the interspacecraft correlation could be less significant for events with stronger fluctuations (indicated by the greater σ_{Bx} values).

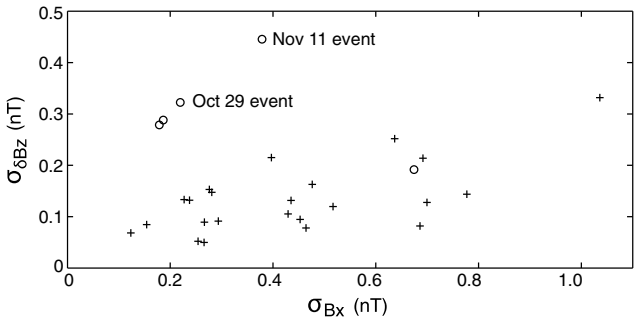

Figure 6. A scatter plot of 23 nonlunar lobe events listed in Table 1, each represented by a plus sign, identified by ARTEMIS dual-probe observations. The abscissa of each plus sign corresponds to the B_x standard deviation (average of P1 and P2 data) within the 1 h interval, and the ordinate is the standard deviation of the interspacecraft magnetic differences δB_z. Also shown are five circles representing these parameters obtained from the lunar flyby events listed in Table 2, which include the two benchmark events on 11 November 2011 and 29 October 2012.

We will next show that the $\sigma_{\delta Bz}$ values in these nonlunar lobe events were generally lower than those in the lunar flyby events. We utilize the same ARTEMIS 2 year data to find all of the lunar flyby events with similar configurations to the two benchmark events, having one probe orbiting across the lunar-connected flux tubes at low altitude and the other at the unperturbed

Table 2. List of Lunar Flyby Lobe Events

Event #	Date	Interval Midpoint	σ_{Bx} at P1 (nT)	σ_{Bx} at P2 (nT)	$\sigma_{\delta Bz}$ (nT)
1[a]	2011-10-13	11:59:41	0.17	0.19	0.28
2[a]	2011-11-11	11:07:07	0.42	0.34	0.45
3	2012-02-07	02:53:52	0.68	0.67	0.19
4[a]	2012-10-29	04:55:21	0.24	0.20	0.32
5[a]	2012-10-30	08:35:48	0.17	0.20	0.29

[a]Events with upward-moving lunar heavy ions.

lobe at least 6000 km from the Moon in *Y*. Similarly, during the 1 h interval centered at the closest approach of the first probe's footprint to the lunar center, we require that the absolute value of the 60 s running-averaged B_x time derivative be always smaller than 0.01 nT/s at both probes and that the background plasma beta be always smaller than 0.1 at the probe unconnected with the lunar flux tubes. Five events listed in Table 2, including the two already studied (events 2 and 4 in Table 2), satisfy these criteria. Events 1, 2, 4, and 5 showed clear signatures of heavy ions moving away from the Moon, and they all have relatively low σ_{Bx} but significantly higher $\sigma_{\delta Bz}$ values (shown as circles in Figure 6) than nonlunar events. The only exception, event 3 on 07 February 2012 with no lunar ions observed, has a low $\sigma_{\delta Bz}$ value of 0.19 comparable with nonlunar events. The distinct separation between these different kinds of events, therefore, supports the argument that the δB_z variations are indeed signatures of lunar-associated field-aligned current in these lunar flybys. Even though the data set is small, the separation also implies an association between lunar heavy ions and field-aligned currents.

6. Summary and Discussion

We present observations of two events in the terrestrial magnetotail lobe, both characterized by the presence of heavy ions of lunar origin at the ARTEMIS probe that was magnetically connected with the sunlit lunar surface. We utilize the ARTEMIS mission's unprecedented dual-probe observations, by treating the magnetic measurements at the other ARTEMIS probe as background lobe fields, to obtain the background-subtracted magnetic perturbations when the first probe moved in the dawn-dusk direction across flux tubes magnetically connected to the Moon. The perturbations, most significantly in B_z, are clear indications of field-aligned current above the lunar dayside surface.

We then examine the carriers of field-aligned current. Despite the widespread expectation that in any space plasma environment field-aligned current should be carried only by electrons because of their high mobility, in these two cases, the contribution from ions of lunar origin should not be neglected. Heavy lunar ions, repelled from the Moon by the near-surface electric field, carry a field-aligned earthward current of $\sim$0.5 nA/m^2, a number on the same scale as the current density required (but still insufficient) to produce the observed magnetic perturbations. Such new charging currents should be considered in the future studies of lunar surface charging and associated electrostatic potential profiles.

We also find that the current contribution from electrons shows various features at different energies. The field-aligned current carried by electrons at energies above 100 eV can be negligible (as in the 11 November event) because of the scarcity of high-energy electrons in the lobe, or can be in the earthward direction (as in the 29 October event) because of lunar blockage of earthward moving electrons. Electrons at lower energies, on the other hand, can carry stronger field-aligned current than the ion current and the high-energy electron current combined. The current direction, however, can be either earthward (as in the 11 November event) or tailward (as in the 29 October event).

The nonzero net current, responsible for the magnetic field perturbations observed by ARTEMIS, suggests that the lunar surface charging process and the associated plasma environment may not be treated as a one-dimensional current balance problem as usually assumed [*Nitter et al.*, 1998; *Farrell et al.*, 2013; *Stubbs et al.*, 2014]. Provided that an equilibrium state can be achieved within few electron plasma periods, the persistent observations of nonzero field-aligned current suggest that the established equilibrium is probably three-dimensional so field-aligned current closure can still be achieved through the other directions.

The current in the *Y* or *Z* directions could arise from the difference between ion and electron motion on ion gyroradius scales, given that heavy ions of lunar origin could have gyroradii comparable with the lunar radius (for example, a 150 eV Si^+ in a field of 10 nT has a gyroradius of 940 km). In the two events analyzed, the lunar ions also carried a current of $\sim$0.5–1 nA/m^2 in the duskward direction (not shown), which

is comparable to or sometimes even greater than the ion-carried J_x and should contribute to the magnetic perturbations in the lunar space environment. Unfortunately, in these two events, probe motion (mostly along the *Y* direction) did not allow a J_y integration to estimate the associated magnetic perturbations. A more systematic study is required to evaluate the roles of these local currents in the lunar dayside magnetic and plasma environment.

It is also probable that ions of lunar origin can affect electron motion in the lunar dayside environment, given that the electron density can be significantly enhanced to maintain quasi-neutrality in the presence of these heavy ions [*Zhou et al.*, 2013]. We also expect that these electrons could be accelerated toward the bulk of the heavy ions in either direction along the field line. This could explain the different directions of low-energy electron motion in the two events. Better understanding of these dynamic processes in the lunar dayside environment requires further analysis of the ARTEMIS data as well as theoretical studies and numerical simulations, with the roles of lunar heavy ions and their accompanying electrons in multispecies plasma dynamics taken into account.

Acknowledgments

The ARTEMIS mission is operated under NASA contract NAS5-02099. We are especially grateful to J.P. McFadden, U. Auster, and F. Plaschke for providing support on the usage of the ARTEMIS ESA and FGM data. We also thank J. Lewis and P. Cruce for software development and assistance, and J. Hohl for editorial support.

Yuming Wang thanks the reviewers for their assistance in evaluating this paper.

References

Angelopoulos, V. (2008), The THEMIS mission, *Space Sci. Rev.*, *141*, 5–34.
Angelopoulos, V. (2011), The ARTEMIS mission, *Space Sci. Rev.*, *165*, 3–25, doi:10.1007/s11214-010-9687-2.
Auster, H. U., et al. (2008), The THEMIS fluxgate magnetometer, *Space Sci. Rev.*, *141*, 235–264.
Bonnell, J. W., F. S. Mozer, G. T. Delory, A. J. Hull, R. E. Ergun, C. M. Cully, V. Angelopoulos, and P. R. Harvey (2008), The electric field instrument (EFI) for THEMIS, *Space Sci. Rev.*, *141*, 303–341.
Farrell, W. M., A. R. Poppe, M. I. Zimmerman, J. S. Halekas, G. T. Delory, and R. M. Killen (2013), The lunar photoelectron sheath: A change in trapping efficiency during a solar storm, *J. Geophys. Res. Planets*, *118*, 1114–1122, doi:10.1002/jgre.20086.
Fu, J. H. M. (1971), Surface potential of a photoemitting plate, *J. Geophys. Res.*, *76*, 2506–2509, doi:10.1029/JA076i010p02506.
Goldstein, B. E. (1974), Observations of electrons at the lunar surface, *J. Geophys. Res.*, *79*, 23–35, doi:10.1029/JA079i001p00023.
Guernsey, R. L., and J. H. M. Fu (1970), Potential distribution surrounding a photo-emitting, plate in a dilute plasma, *J. Geophys. Res.*, *75*, 3193–3199, doi:10.1029/JA075i016p03193.
Halekas, J. S., G. T. Delory, R. P. Lin, T. J. Stubbs, and W. M. Farrell (2008), Lunar Prospector observations of the electrostatic potential of the lunar surface and its response to incident currents, *J. Geophys. Res.*, *113*, A09102, doi:10.1029/2008JA013194.
Halekas, J. S., G. T. Delory, W. M. Farrell, V. Angelopoulos, J. P. McFadden, J. W. Bonnell, M. O. Fillingim, and F. Plaschke (2011), First remote measurements of lunar surface charging from ARTEMIS: Evidence for nonmonotonic sheath potentials above the dayside surface, *J. Geophys. Res.*, *116*, A07103, doi:10.1029/2011JA016542.
Harada, Y., S. Machida, J. S. Halekas, A. R. Poppe, and J. P. McFadden (2013), ARTEMIS observations of lunar dayside plasma in the terrestrial magnetotail lobe, *J. Geophys. Res. Space Physics*, *118*, 1–13, doi:10.1002/jgra.50296.
Hilchenbach, M., D. Hovestadt, B. Klecker, and E. Möbius (1993), Observation of energetic lunar pick-up ions near Earth, *Adv. Space Res.*, *13*, 321–324.
Li, S.-S., V. Angelopoulos, A. Runov, S. A. Kiehas, and X.-Z. Zhou (2013), Plasmoid growth and expulsion revealed by two-point ARTEMIS observations, *J. Geophys. Res. Space Physics*, *118*, 2133–2144, doi:10.1002/jgra.50105.
Mall, U., E. Kirsch, K. Cierpka, B. Wilken, A. Söding, F. Neubauer, G. Gloeckler, and A. Galvin (1998), Direct observation of lunar pick-up ions near the Moon, *Geophys. Res. Lett.*, *25*, 3799–3802, doi:10.1029/1998GL900003.
McFadden, J. P., C. W. Carlson, D. Larson, V. Angelopolos, M. Ludlam, R. Abiad, and B. Elliot (2008a), The THEMIS ESA plasma instrument and in-flight calibration, *Space Sci. Rev.*, *141*, 277–302.
McFadden, J. P., C. W. Carlson, D. Larson, J. Bonnell, F. Mozer, V. Angelopoulos, K.-H. Glassmeier, and U. Auster (2008b), THEMIS ESA first science results and performance issues, *Space Sci. Rev.*, *141*, 477–508, doi:10.1007/s11214-008-9433-1.
Nitter, T., O. Havnes, and F. Melandsø (1998), Levitation and dynamics of charged dust in the photoelectron sheath above surfaces in space, *J. Geophys. Res.*, *103*, 6605–6620, doi:10.1029/97JA03523.
Poppe, A., and M. Horányi (2010), Simulations of the photoelectron sheath and dust levitation on the lunar surface, *J. Geophys. Res.*, *115*, A08106, doi:10.1029/2010JA015286.
Poppe, A., J. S. Halekas, and M. Horányi (2011), Negative potentials above the day-side lunar surface in the terrestrial plasma sheet: Evidence of non-monotonic potentials, *Geophys. Res. Lett.*, *38*, L02103, doi:10.1029/2010GL046119.
Poppe, A. R., R. Samad, J. S. Halekas, M. Sarantos, G. T. Delory, W. M. Farrell, V. Angelopoulos, and J. P. McFadden (2012), ARTEMIS observations of lunar pick-up ions in the terrestrial magnetotail lobes, *Geophys. Res. Lett.*, *39*, L17104, doi:10.1029/2012GL052909.
Poppe, A. R., J. S. Halekas, R. Samad, M. Sarantos, and G. T. Delory (2013), Model-based constraints on the lunar exosphere derived from ARTEMIS pickup ion observations in the terrestrial magnetotail, *J. Geophys. Res. Planets*, *118*, 1135–1147, doi:10.1002/jgre.20090.
Slavin, J. A., E. J. Smith, B. T. Tsurutani, D. G. Sibeck, H. J. Singer, D. N. Baker, J. T. Gosling, E. W. Hones, and F. L. Scarf (1984), Substorm associated traveling compression regions in the distant tail-ISEE-3 geotail observations, *Geophys. Res. Lett.*, *11*, 657–660.
Slavin, J. A., et al. (1999), Dual spacecraft observations of lobe magnetic field perturbations before, during and after plasmoid release, *Geophys. Res. Lett.*, *26*, 2897–2900.
Stubbs, T. J., W. M. Farrell, J. S. Halekas, J. K. Burchill, M. R. Collier, M. I. Zimmerman, R. R. Vondrak, G. T. Delory, and R. F. Pfaff (2014), Dependence of lunar surface charging on solar wind plasma conditions and solar irradiation, *Planet. Space Sci.*, *90*, 10–27, doi:10.1016/j.pss.2013.07.008.
Tanaka, T., et al. (2009), First in situ observation of the Moon-originating ions in the Earth's Magnetosphere by MAP-PACE on SELENE (KAGUYA), *Geophys. Res. Lett.*, *36*, L22106, doi:10.1029/2009GL040682.
Walbridge, E. (1973), Lunar photoelectron layer, *J. Geophys. Res.*, *78*, 3668–4005, doi:10.1029/JA078i019p03668.
Whipple, E. C. (1981), Potentials of surfaces in space, *Rep. Prog. Phys.*, *44*, 1197–1250, doi:10.1088/0034-4885/44/11/002.
Yokota, S., et al. (2009), First direct detection of ions originating from the Moon by MAP-PACE IMA onboard SELENE (KAGUYA), *Geophys. Res. Lett.*, *36*, L11201, doi:10.1029/2009GL038185.
Zhou, X.-Z., V. Angelopoulos, A. R. Poppe, and J. S. Halekas (2013), ARTEMIS observations of lunar pick-up ions: Mass-constraints on ion species, *J. Geophys. Res. Planets*, *118*, 1766–1774, doi:10.1002/jgre.20125.